Seismic attenuation in glacial ice: A proxy for englacial temperature

L. E. Peters,[1,2] S. Anandakrishnan,[1,2] R. B. Alley,[1,2] and D. E. Voigt[1,2]

Received 25 August 2011; revised 5 February 2012; accepted 21 February 2012; published 12 April 2012.

[1] Seismic attenuation α, or internal friction Q^{-1}, in glacial ice is highly sensitive to temperature, particularly near the melting point. Here we detail a technique to estimate Q and apply it to active source seismic data from Jakobshavn Isbrae, Greenland. We compare our results to measured and modeled temperature profiles of the ice in the region. We find an excellent match, with differences between seismically estimated and modeled temperatures of less than 2°C. Mapping variations in seismic Q through glacial ice thus is shown to allow detailed estimation of englacial temperature profiles, which may be of special value in regions where in situ measurements are logistically difficult.

Citation: Peters, L. E., S. Anandakrishnan, R. B. Alley, and D. E. Voigt (2012), Seismic attenuation in glacial ice: A proxy for englacial temperature, *J. Geophys. Res.*, *117*, F02008, doi:10.1029/2011JF002201.

1. Introduction

[2] Flow of glaciers and ice sheets is strongly affected by their thermal regime, with warmer ice deforming more rapidly, and the onset of melting greatly increasing basal velocity [e.g., *Hooke*, 1981; *Huybrechts and Oerlemans*, 1988]. Accurate knowledge of the thermal regime thus will allow more accurate modeling of the evolution of the Earth's ice sheets, improving projections on how they will respond to anthropogenic forcing in the future.

[3] The thermal regime of ice reflects a complex interplay between the downward advection of surface cold through accumulation, horizontal advection via ice flow, geothermal flux from the geology beneath, and frictional heating due to ice deformation and basal sliding [e.g., *Cuffey and Paterson*, 2010]. Specialized models have been developed to better understand these effects [*Robin*, 1955; *Weertman*, 1968; *Paterson and Clarke*, 1978; *Funk et al.*, 1994; *Dahl-Jensen et al.*, 1998], leading to improved thermomechanical ice sheet models [e.g., *Greve*, 1997; *Payne et al.*, 2000; *Parizek et al.*, 2005].

[4] The distribution of frozen and thawed beds is of particular importance. Regions where the bed is near but below the pressure melting point may be most subject to rapid acceleration of ice flow if the bed warms in the future, whereas thawed regions lacking sufficient heat input may be prone to deceleration [e.g., *Parizek and Alley*, 2004; *Joughin et al.*, 2005].

[5] Direct measurements of englacial temperature in polar ice sheets are largely restricted to a handful of locations, typically associated with ice cores from the interior ice divides and domes of Antarctica and Greenland, along with limited observations along fast-flowing glaciers and ice streams [e.g., *Iken et al.*, 1993; *Engelhardt*, 2004]. Additional measurements are currently limited by the logistical requirements involved with obtaining in situ measurements of englacial temperature. Here, we present a novel approach for constraining englacial temperature through an ice sheet by active seismic methods, much more rapidly and cheaply than typically possible with drilling. By utilizing the spectral ratio method [e.g., *Tonn*, 1991; *Dasgupta and Clark*, 1998], we estimate seismic attenuation through the ice column, which in turn yields the temperature of the ice.

2. Seismic Theory

[6] Consider a seismic source wavelet of amplitude A_0 that travels through the ice and is recorded at a horizontal distance x from the source location. The seismic wave may travel directly from the source to the receiver without undergoing reflection (the so-called "direct wave", which we treat separately below). Alternatively, the wavelet may follow a raypath of length $r(x)$, which includes a reflection off a subsurface horizon with reflectivity $R(x)$ (the horizon is assumed to have an offset-dependent reflection coefficient); its recorded amplitude is

$$A(x) = A_0 R(x) G(x) e^{-\alpha(f) r(x)}, \tag{1}$$

where the geometric spreading factor $G(x)$ accounts for spreading losses along the raypath [e.g., *Aki and Richards*, 2002]. The interface reflectivity $R(x)$ is determined by the elastic properties on either side of the interface (primarily the compressional wave velocity V_P, shear wave velocity V_S, and density ρ). The remaining parameter $\alpha(f)$ is the *frequency-dependent* anelastic seismic attenuation, and is a measure of how rapidly the seismic wave attenuates due to the internal friction of the medium.

[1]Department of Geosciences, Pennsylvania State University, University Park, Pennsylvania, USA.
[2]Earth and Environmental Systems Institute, Pennsylvania State University, University Park, Pennsylvania, USA.

0148-0227/12/2011JF002201

[7] Attenuation α is sensitive to parameters such as lithology, anisotropy, fluid content, and porosity [e.g., *Töksoz and Johnston*, 1981], although as discussed below, temperature is the most important control on seismic attenuation in ice. The internal friction leads to the damping of free oscillations of a propagating seismic wave, converting some fraction of the seismic energy to heat along interfaces in the medium. Seismic attenuation α is often expressed in a nondimensional form as the seismic quality factor Q, or internal friction Q^{-1}. The relationship between Q and α is

$$Q = \frac{\pi f}{V_P \alpha(f)}, \tag{2}$$

where f is frequency of the seismic wavelet and V_P is the compressional wave seismic velocity of the attenuating medium [e.g., *Aki and Richards*, 2002]. Over seismic frequencies (approximately 10 to 10^3 Hz) the attenuation, α, increases approximately linearly with frequency [e.g., *Tonn*, 1991; *Aki and Richards*, 2002]. Thus Q is effectively *frequency independent.* This assumption is commonly made in seismology and is appropriate for our data, where the data have been filtered to a band between 120 and 280 Hz. Note that in equation (2), higher Q equates to lower attenuation α and vice versa.

[8] *Töksoz and Johnston* [1981] summarized data on seismic attenuation for various earth materials and subsurface conditions. In general, unfractured crystalline rocks have higher Q values ($Q > 500$) than porous or fractured media ($Q < 100$), in which there is greater frictional heating and fluid motion. Laboratory studies have shown that Q increases with increasing pressure due to microcrack closure [e.g. *Töksoz et al.*, 1979]. The effect of fluids on Q is variable, with dry rocks generally having higher Q values than wet rocks. The initial wetting of the rock causes a decrease in Q as the fluid lubricates cracks and grain boundaries, aiding in frictional sliding [e.g., *Mavko and Nur*, 1979]; partial saturation of the rock also lowers Q through dissipation by free fluid flow in the pore space in response to excitation from the propagating seismic wave. However, full saturation of the pore space can restrict this flow and lead to an increase in Q to values comparable to those observed in the dry material [e.g., *Mavko and Nur*, 1979]. Seismic anisotropy due to oriented cracks, microfractures, laminae, or crystal orientation leads to an associated attenuation anisotropy. In general, seismic attenuation is at a minimum when the seismic wave propagation is parallel to the primary axis of anisotropy [e.g., *Best et al.*, 2007; *Chinchinina et al.*, 2009].

[9] Finally, and most significantly for glaciological applications, seismic attenuation exhibits a strong temperature dependence, particularly when the attenuating medium approaches its bulk melting point. Experimental studies of Q in mantle materials highlight the sensitivity of Q to temperature at the onset of partial melting [e.g., *Artemieva et al.*, 2004], where Q^{-1} appears to follow an Arrhenius relationship at seismic frequencies and increases exponentially with temperature [e.g., *Jackson et al.*, 1992; *Artemieva et al.*, 2004; *Matas and Bukowinski*, 2007]. Similarly, laboratory experiments utilizing an ice-brine binary system showed low attenuation (high Q) when fully frozen, increasing attenuation with increasing temperature, and a jump in Q at the eutectic temperature due to the onset of melt [*Spetzler and Anderson*, 1968; see also *Matsushima et al.*, 2008].

3. Seismic Attenuation in Glacial Ice

[10] Internal friction in ice Q^{-1}, and thus seismic attenuation α, arises from several energy loss mechanisms at scales ranging from the molecular to the grain scale, each exhibiting a marked sensitivity to temperature (Figure 1). For single-crystal ice, the dominant mechanism at seismic frequencies is a Debye-type relaxation due to the realignment of water molecules [e.g., *Kuroiwa and Yamaji*, 1959; *Kuroiwa*, 1964].

[11] Because this mechanism is intrinsic to all ice crystals, it is part of all attenuation spectra, and typically becomes the dominant mechanism for all glacial ice where $T \leq -30°\mathrm{C}$ (Figure 1). At these colder temperatures, c axis fabric can have a significant effect on seismic attenuation, dependent on the angle between the propagating direction of the seismic wave and the c axis (see *Kuroiwa* [1964] and *Oguro et al.* [1982] for a detailed discussion on this topic). In warmer glacial environments, such as many mountain glaciers, the outlet glaciers of Greenland and West Antarctica, and the periphery of East Antarctica, grain boundary processes dominate the variability in Q, as discussed below.

[12] For polycrystalline ice, which includes all naturally occurring glacier ice, quasi-liquid films generated by melting at grain boundaries dominate seismic attenuation when they are present; the temperature above which melt occurs for glacial ice is approximately $T = -30°\mathrm{C}$ [e.g., *Dash et al.*, 1995, 1996] (Figure 1), but can be lowered by sufficiently high concentrations of impurities [*Kuroiwa and Yamaji*, 1959; *Kuroiwa*, 1964; *Spetzler and Anderson*, 1968; *Matsushima et al.*, 2008]. This grain boundary water film causes an approximate exponential increase in internal friction Q^{-1} with temperature across all frequencies [*Kuroiwa*, 1964] and dominates relative to other causes at sufficiently high temperatures.

[13] Field studies of seismic attenuation in glacial ice have used near-surface measurements (i.e., direct-wave arrivals) to estimate attenuation in the upper 10s to 100s of meters of the ice [*Millecamps and Lafargue*, 1957; *Westphal*, 1965; *Brockamp and Kohnen*, 1965; *Langleben*, 1969; *Clee et al.*, 1969; *Kohnen*, 1969; *Bentley and Kohnen*, 1976; *Gusmeroli et al.*, 2010]. Estimates of attenuation through the ice column have used the strong basal reflections [*Robin*, 1958; *Jarvis and King*, 1993] and prominent deep englacial reflections [*Bentley*, 1971a]. Table 1 summarizes the results of these studies, with all observed attenuation values converted to Q. It should be noted that the frequency range for these analyses extends from the ultrasonic [*Millecamps and Lafargue*, 1957; *Westphal*, 1965; *Langleben*, 1969] to the seismic frequencies [*Robin*, 1958; *Brockamp and Kohnen*, 1965; *Clee et al.*, 1969; *Kohnen*, 1969; *Bentley*, 1971a; *Bentley and Kohnen*, 1976; *Jarvis and King*, 1993; *Gusmeroli et al.*, 2010]; caution is advisable in comparisons across this data set because Rayleigh-type scattering controls attenuation losses in the kilohertz range where wavelengths are on the order of the grain size, whereas internal friction dominates at lower frequencies ($10 - 10^3$ Hz) due to grain boundary and intragranular processes. Nevertheless, it appears that the various studies

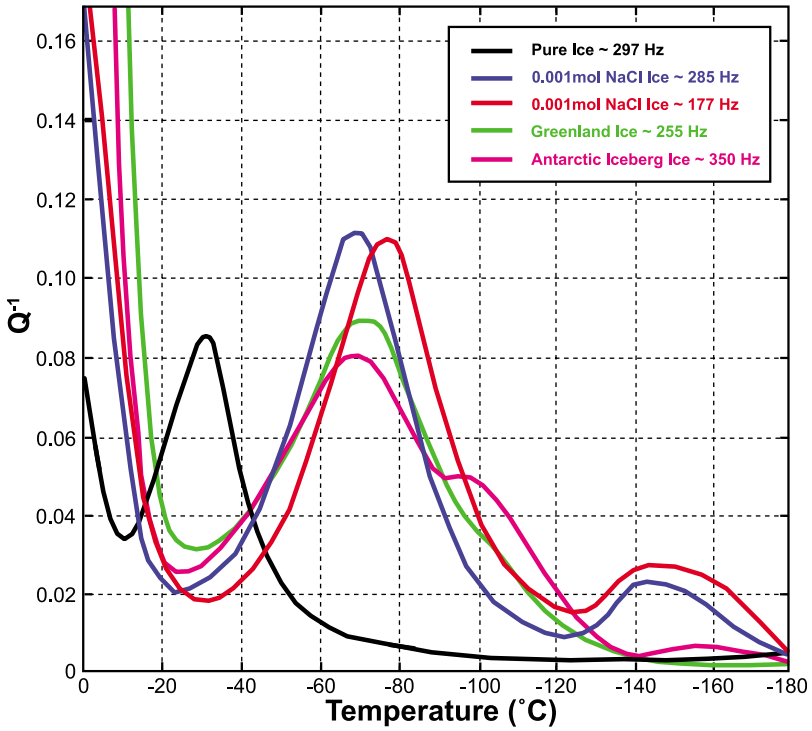

Figure 1. Relaxation spectra of ice versus temperature, adapted from *Kuroiwa* [1964]. These curves demonstrate how internal friction Q^{-1} in ice varies with temperature. The relaxation spectra for polycrystalline ice samples from various locations and impurity concentrations [*Kuroiwa*, 1964] are shown. At warmer temperatures ($T > -30°C$), grain boundary friction dominates; chemical impurities shift this attenuation process to colder temperatures. The prominent relaxation peaks observed in each sample in the $-40°C$ to $-100°C$ range are the result of proton movement in the water molecules.

of seismic attenuation point to a strong increase of Q^{-1} with temperature.

4. Data Collection and Analysis

[14] In May 2007, a wide-angle (incidence angles at the base of the ice ranging from normal to >45°), common midpoint (CMP) seismic reflection experiment was performed in the accumulation zone of Jakobshavn Isbrae, Greenland, approximately 100 km inland of the grounding line (Figure 2). The receiver array consisted of 24 single-component geophones at a 20 m spacing. The sensors were 1 m long rods containing four equally spaced 40 Hz elements oriented vertically (dubbed "georods"), extending one meter below the surface. One-kilogram explosive charges were used as sources, detonated 10 m below the surface. Source-to-receiver offsets ranged from 0 m to 4000 m.

[15] The resultant seismic data were collected via a wide-angle reflection experiment, whereby the same 240 m segment of the subsurface was imaged over all source-to-receiver offsets (Figure 3). The experiment begins with the seismic source detonated 0 m from the end of the 460 m receiver array, with the source and first receiver located at 0 m. We then move the seismic source location by +240 m and the

Table 1. Seismic Attenuation Calculations Through Ice in Various Glaciated Regions, Given in Terms of the Seismic Quality Factor Q[a]

Location	Surface Temperature (°C)	Quality Factor (Q)	Frequency Range (Hz)	Range of Ice Column Sampled	Reference
Mer de Glace, France	−5	155–180	65000	upper 30 m	*Millecamps and Lafargue* [1957]
Blue Glacier, Washington, USA	0	150	2500	upper 60 m	*Westphal* [1965]
Tanquary Fiord, Ellesmere,		150	100000		
Ellesmere Island, Canada	−10	<110	500000	1–5 m sea ice	*Langleben* [1969]
Larsen Ice Shelf, Antarctic Peninsula	−10 to −12	50–160	60–90	entire ice column	*Jarvis and King* [1993]
West Antarctica	−14 to −25	400–670	100–200	entire ice column	*Bentley* [1971a]
Greenland Ice Sheet	−22	500	100–150	80+% of the ice column	*Brockamp and Kohnen* [1965]
Queen Maud Land, East Antarctica	−38	260–390	80–130	entire ice column	*Robin* [1958]
Storglaciären, Sweden	−1	7–9	100–300	upper 10–20 m	*Gusmeroli et al.* [2010]
Athabasca Glacier, Alberta, Canada	0	60–70	120–1000	upper 100 m	*Clee et al.* [1969]
Greenland Ice Sheet	>−20	115–190	50–100	upper 100–500 m	*Kohnen* [1969]
Byrd Station, West Antarctica	−28	550–1000	136	upper 100–500 m	*Bentley and Kohnen* [1976]

[a]The first three measurements, utilizing ultrasonic frequencies, capture seismic energy loss effects largely due to scattering. The next four measurements are from the bulk ice column at each location sampled. The last four measurements focus on the upper ice column at each location.

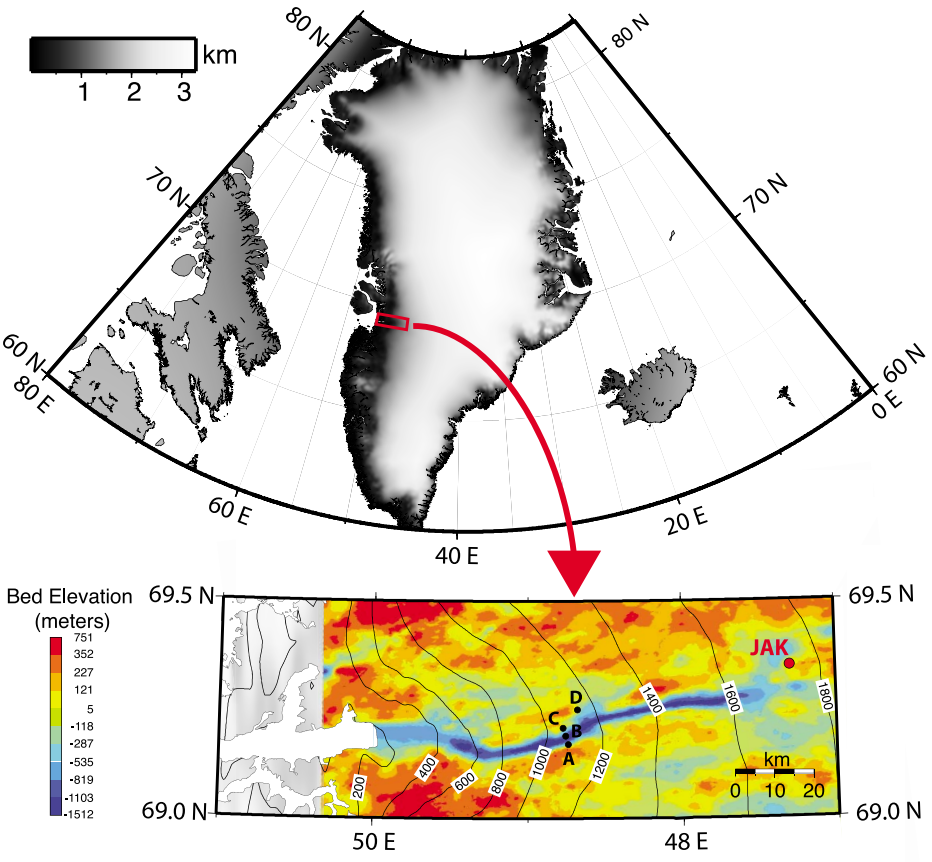

Figure 2. Location map of the seismic study, modified from *Horgan et al.* [2008]. (top) Surface elevations for the Greenland ice sheet [*Bamber et al.*, 2001] and location of the detailed map (red box). (bottom) Detailed map of Jakobshavn Isbrae with surface elevation (contours) [*Bamber et al.*, 2001] and subglacial topography (CReSIS bed elevation map, derived from ice-penetrating radar; data can be found at https://www.cresis.ku.edu/data), along with the locations of this seismic study (red circle JAK) and previous englacial temperature measurements (black circles A–D [*Iken et al.*, 1993; *Lüthi et al.*, 2002]).

receiver array by −240 m, detonate the source and image the same region of the subsurface. We continuethis process, moving the source and receiver array outward in 240 m increments, to continuously image a 240 m section of the subsurface from 0 m to 4000 m source-to-receiver offset. This repeated sampling of the subsurface is key to constraining seismic properties, in this case attenuation α, via the spectral ratio method [e.g., *Tonn*, 1991].

[16] Strong ice bottom and englacial reflections are clearly observed across our data set, along with the direct arrival (Figure 3). Eight distinct englacial reflections are observed within the ice column, with the uppermost reflector at a depth of z = 970 m or a normalized depth of Z = 0.57 (the total ice thickness is h = 1693 m), labeled *R*970 in Figure 3. These englacial reflections arise from a contrast in seismic properties within the ice column. Since the density of the ice remains quite constant below the firn-ice transition, these reflections are primarily due to changes in seismic wave velocity (V_P: compressional wave seismic velocity, and/or V_S: shear wave seismic velocity); these changes are indicative of changes in crystal-orientation fabric, where seismic velocity variations of <1% can often be detected [*Bennett*, 1968; *Bentley*, 1971b; *Blankenship and Bentley*, 1987; *Horgan et al.*, 2008, 2011].

[17] No filtering or processing have been applied to the seismic data used in the spectral analysis in order to preserve the true amplitudes of observed wavelets from each englacial reflection and the ice bottom reflector. However, standard processing techniques have been applied to Figure 3 to better display the reflectors chosen for our seismic analysis. Bandpass filters, dip filters, and FK filters were applied to remove some of the surface-generated noise from our data. Automatic gain control was also applied to strengthen each reflector relative to the background noise. A normal moveout correction was then performed to flatten the englacial and ice bottom seismic reflections displayed. Since no processing was applied to the seismic data in our analysis, we chose to delete traces in which excessive interference from surface waves or the direct arrival was present.

[18] We used the spectral ratio method of *Dasgupta and Clark* [1998] to determine Q for each observed seismic signal. This method involves analyzing the ratio of the frequency spectra of the source wavelet A_0 and the recorded wavelet $A(x)$ at each offset x (Figure 4; spectral analysis of the ice bottom

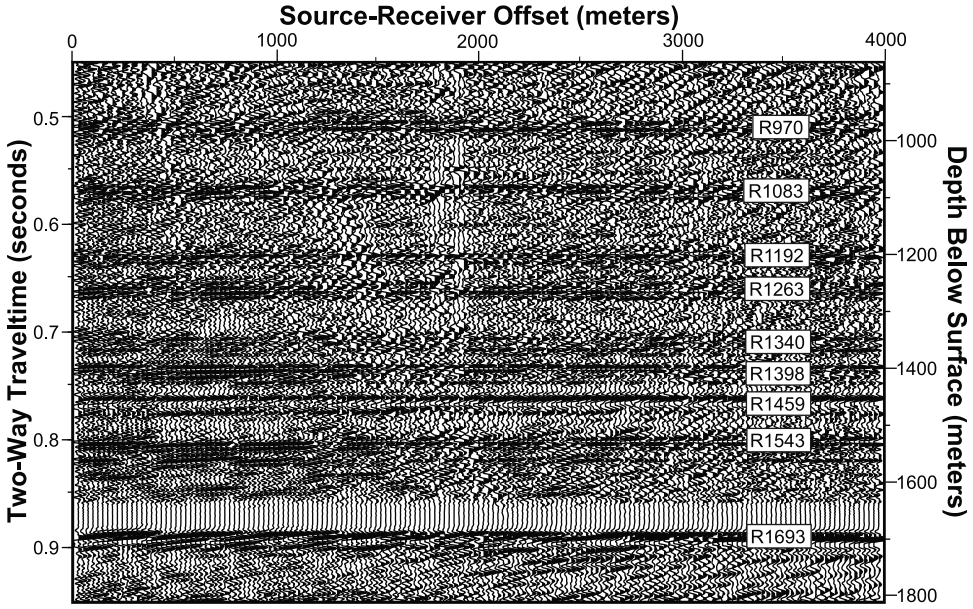

Figure 3. The wide-angle seismic common midpoint (CMP) gather collected at the JAK location. The data have been processed to highlight the englacial reflectors and to remove surface-generated noise; band-pass filtering, dip filtering, and FK filtering have been applied along with automatic gain control, and a normal moveout correction has been performed to flatten these reflectors. Some surface noise can still be observed within the data set, particularly in the 500–2000 m offset range for the englacial reflectors. The eight englacial reflectors and the ice bottom are labeled on the basis of their respective depths beneath the surface.

reflector $R1693$ is highlighted here). Rearranging equation (1) in terms of Q results in the spectral ratio [e.g., *Tonn*, 1991; *Dasgupta and Clark*, 1998]

$$\log\frac{A(x)}{A_0} = -\frac{\pi f}{QV_P}r(x) + \log[R(x)G(x)]. \tag{3}$$

Here the frequency spectra of the source wavelet (Figure 4a) and the wavelets at each offset x for the direct arrival, the englacial reflectors, and the ice bottom (ice bottom R1693 is shown in Figure 4b) are calculated, taking a $\pm$30 msec window surrounding each wavelet. The source wavelet A_0 is estimated from a georod 60 m from the source (Figure 4a), as closer georods had clipped waveforms. From equation (3), there is a linear relationship between the spectral ratio and frequency f at each offset x, with slope

$$\gamma(x) = -\frac{\pi}{QV_P}r(x). \tag{4}$$

We assume that $G(x)$ and $R(x)$ are *frequency independent*, since the spreading loss parameter $G(x)$ is solely a function of the path along which the seismic wave propagates and the reflection coefficient $R(x)$ is determined by the elastic properties (V_P, V_S, ρ) at the seismic interface, all of which are likely insensitive to frequency in the band of interest. For our data set, we limited our spectral ratio analysis to a frequency bandwidth of $f = 120-280$ Hz, as this range contains most of the seismic energy observed within all of our selected seismic wavelets (Figure 4c). Thus $\gamma(x)$ is derived for the spectral ratio of at each offset x.

[19] For a constant V_P in the ice, $r(x) = x$ for the direct arrival and $r(x) = 2\sqrt{\frac{x^2}{2} + h^2}$ for a seismic reflection (where h is the depth to the reflector). However, V_P in general is not constant because of the low-density firn, anisotropy in the ice, and the temperature dependence of seismic velocity [*Bentley*, 1971b; *Kohnen*, 1974; *Blankenship and Bentley*, 1987]. We follow *Gusmeroli et al.* [2010], and use the travel time difference $\delta t = t(x) - t_0$ between our source wavelet at time t_0 and the arrival time $t(x)$ of our recorded wavelet at offset x as a proxy for $r(x)/V_P$ in equation (4). Thus,

$$\gamma(\delta t) = -\frac{\pi\delta t}{Q}, \tag{5}$$

where $\gamma(\delta t)$ is calculated for a particular offset x and its associated traveltime difference δt in our CMP gather [*Gusmeroli et al.*, 2010]. The slope of this linear regression is then used to determine Q (Figure 4d).

[20] For the direct arrival, the Q we determine from equation (5) is for the region below the firn, in the upper ice column, where the seismic waves sample depths of approximately 150–200 m [*Spetzler and Sneider*, 2004]. This direct arrival is the first seismic signal observed at our receiver array, as surface waves travel through the firn and upper ice column. At near offsets (<1000 m offset, where the firn is observed to be $\sim$75 m thick in this region, following the shallow seismic approach of *Rothlisberger* [1972] and *Shearer* [2009]), Q analysis via equation (5) will not yield a single or distinct Q; the surface waves over these near offsets

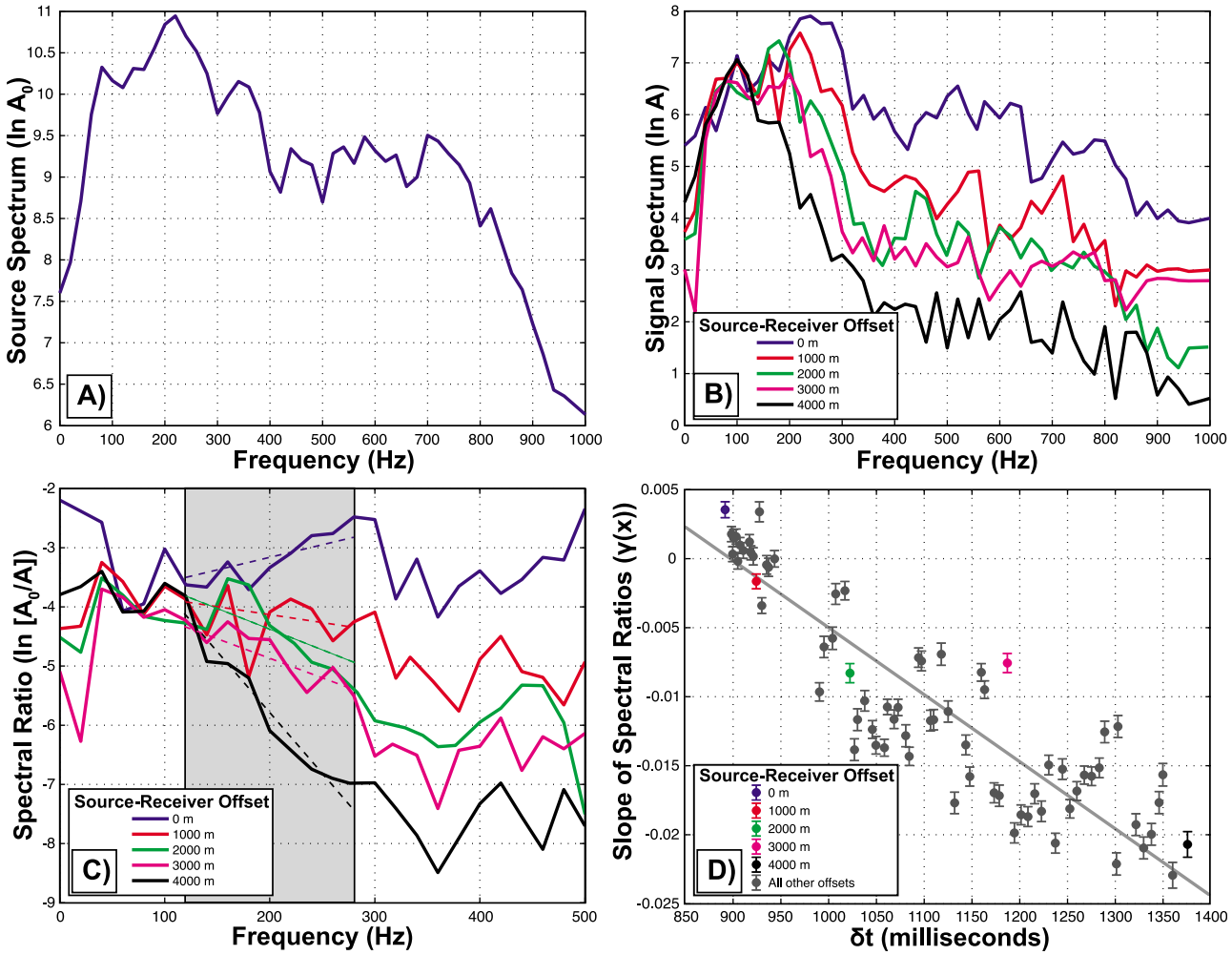

Figure 4. An overview of the spectral ratio method, using the ice bottom reflection ($R1693$ in Figure 3). (a) Frequency spectrum of the source wavelet A_0, taken at 60 m offset from the source. (b) Frequency spectra of the observed signal wavelets from five different source-receiver offsets x. (c) Spectral ratios between the source wavelet (Figure 4a) and the signal wavelet (Figure 4b) from five source-receiver offsets x. The gray box outlines the 120–280 Hz frequency range used for the spectral analysis, following equation (3). The best fitting linear regression for each offset x is shown by a dashed line. The slope of these lines yields $\gamma(x)$ (or $\gamma(\delta t)$). (d) The slope of the spectral ratios $\gamma(x)$ at each observed receiver location x, plotted as a function of δt, the traveltime difference between the source and signal wavelets. The slope of the best fitting line to these $\gamma(\delta t)$ values yields Q, as outlined in equation (5).

are only traveling through the firn itself, with each successive offset dipping a little deeper in the firn, and thus sampling a heterogeneous medium with a nonunique Q. At far offsets (>1000 m offset), these surface waves travel completely though the firn, and refract along the upper ice column. As such, the same region of the upper ice column is sampled with each increasing offset x, yielding a single Q through equation (5).

[21] On the other hand, for the englacial reflectors and ice bottom reflection, the value of Q from equation (5) is an average of $Q(z)$ from the surface down to the the depth z of the reflector.

[22] These depth-averaged Q values can be used to calculate interval values Q_I. For two reflectors at depths z_{n-1} and z_n, with depth-averaged Q values Q_{n-1} and Q_n, respectively, the resultant Q_I for the regions between the two reflectors is [*Dasgupta and Clark*, 1998]

$$Q_I = \frac{t_n - t_{n-1}}{\frac{t_n}{Q_n} - \frac{t_{n-1}}{Q_{n-1}}}, \tag{6}$$

where t_n is the arrival time from horizon n. We then calculated the $Q_I(z)$ profile through the ice column at our seismic site by applying equation (6) to the eight englacial reflectors and ice bottom reflection (Figure 5 and Table 2).

[23] The uncertainties in Q arise from the signal-to-noise ratio (SNR) of each analyzed signal wavelet [*Dasgupta*, 1994] and the goodness of fit of the resultant linear regressions from equations (3) and (5). Given the high SNR in our seismic data, the resultant uncertainties theoretically map to $\sigma_Q \approx 5\%$, as derived from synthetic sensitivity tests [*Dasgupta*, 1994]; these

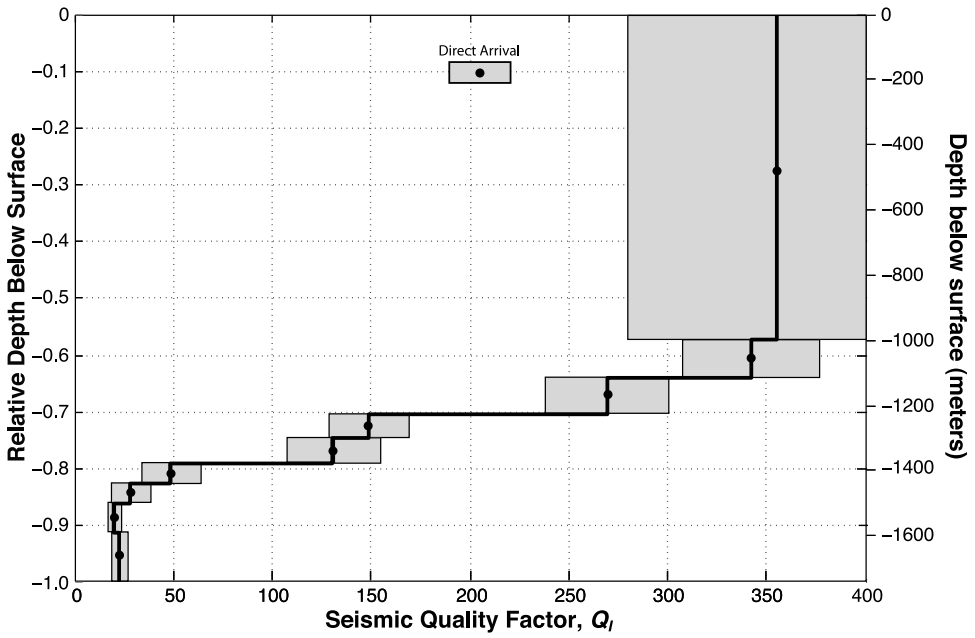

Figure 5. Seismic $Q(z)$ plot as determined from our spectral analysis of the direct arrival, eight englacial reflectors, and ice bottom reflection. Each Q_I gives the average Q value between two reflectors (equation (6)), with the dots showing the center points and uncertainties shown with gray shading (Table 2).

uncertainties are comparable to what we calculated for the lowermost seismic reflectors (Table 2). However, the shallower seismic reflectors possess some traces contaminated with surface wave energy (Figure 3), leading to uncertainties of up to $\sigma_Q = 22\%$ (Table 2). These experimental uncertainties propagate into how welleach linear regression of the spectral ratios fits across our chosen frequency bandwidth in equation (3). Here we have chosen a narrow band of 120–180 Hz, based on an examination of the dominant frequency ($\sim$150 Hz) of our wavelets and of the background noise for each observed reflector and offset (Figure 4b). The uncertainties in Q, in Table 2, are primarily from the uncertainty of the linear regression of $\gamma(\delta t)$.

5. The Temperature Dependence of Q in Ice

[24] As noted above, seismic attenuation in ice is temperature dependent. Here we compare our englacial Q estimates with measurements and models of englacial temperature for Jakobshavn Isbrae. In general, temperature varies vertically within polar glaciers and ice sheets, with the warmest temperatures at the base of the ice. By comparing our determinations of $Q(z)$ with modeled and measured temperature profiles $T(z)$, we show that Q is indeed a good proxy for T (Figure 6).

[25] Temperature profiles were measured about 50 km downglacier of our field site [*Iken et al.*, 1993; *Lüthi et al.*, 2002] at four locations: one in the trunk of the glacier (site B; Figure 2), and three in the shear margin and slow-moving ice nearby (sites A, C, D; Figure 2). A common characteristic of all of these is a relatively cold upper section due to advection of cold surface and upglacier ice [*Dahl-Jensen et al.*, 1998], and a warming toward the bed inresponse to geothermal heat and the energy released by basal sliding and ice deformation [*Iken et al.*, 1993; *Funk et al.*, 1994; *Lüthi et al.*, 2002]. Focusing of heat flow into the deep bedrock trough of the glacier also contributes to the warmth of the deepest ice [*van*

Table 2. Calculated Seismic Q Through the Ice Column on Jakobshavn[a]

Target Signal	Time to Signal (ms)[b]	Depth to Signal (m)	Relative Depth	Q_{RMS}	Q_I	Temperature (°C)
Direct Arrival	$\sim x/3.8$[b]	100–150	0.08–0.12	207±16	207±16	−18.0±0.8
R970	513	970±17	0.57±0.02	355±75	355±75	−21.8±1.6
R1083	572	1083±21	0.64±0.02	353±78	342±36	−21.5±0.9
R1192	630	1192±26	0.70±0.03	343±63	270±32	−19.9±1.0
R1263	665	1263±28	0.75±0.03	324±66	149±20	−15.7±1.1
R1340	705	1340±33	0.79±0.03	293±57	130±24	−14.7±1.4
R1398	732	1398±37	0.83±0.03	243±45	48±15	−7.7±2.3
R1459	762	1459±39	0.86±0.03	187±21	28±10	−3.9±2.6
R1543	804	1543±42	0.91±0.04	142±11	20±3	−1.5±1.2
R1693 (Ice Bottom)	882	1693±49	1.00	94±5	23±4	−2.4±1.3

[a]The temperature values and their uncertainties are derived from equation (7) (Figure 6).

[b]Travel times for the direct arrival exhibit a linear moveout with offset x, following the above equation, where 3.8 m sec^{-1} is the average compressional wave velocity in ice. The travel times for the observed reflectors have normal moveout corrections applied to flatten each reflector to a single time, as shown in Figure 3.

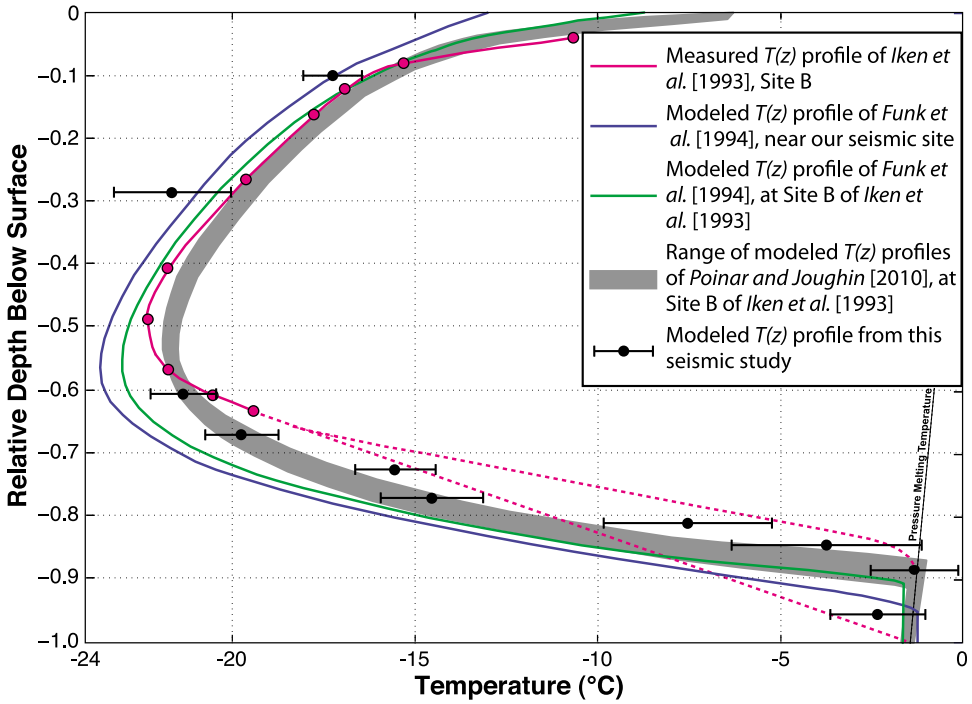

Figure 6. Comparison of our calculated $T(z)$ profile to the englacial temperature observations of *Iken et al.* [1993] and modeled temperature profiles of *Funk et al.* [1994] and *Poinar and Joughin* [2010]. Our $T(z)$ profile is derived from seismic Q measurements following equation (7).

der Veen et al., 2007]. Of particular note is the observation that the glacier and the ice sheet just outside the shear margin have temperate basal ice layers [*Iken et al.*, 1993; *Lüthi et al.*, 2002]. Ice flow modeling confirms the development of this deep temperate layer, and suggests at least some temperate ice may extend upglacier past our site [*Funk et al.*, 1994] [see also *Iken et al.*, 1993; *Lüthi et al.*, 2002; *Poinar and Joughin*, 2010] (Figure 6).

[26] For comparison of the different measured and modeled profiles to our seismic attenuation data, we have normalized all depths to $Z = 0$ at the surface and $Z = 1$ at the bed. Our uppermost englacial seismic reflector then occurs at $Z = 0.57$, at the base of the coldest ice (Figures 5 and 6). Below this, we find a monotonic, exponential downward decrease of Q, consistent with the observed and modeled downward increase in T. Finally, we find that the Q values of the very lowest 14% of the ice are approximately constant, consistent with an isothermal temperate layer [*Iken et al.*, 1993; *Funk et al.*, 1994].

[27] As discussed above, we expect seismic Q to show an Arrhenius-type exponential dependence on temperature. We thus seek a best fit relation between our Q_I values (Figure 5 and Table 2) and the measured temperature values

$$Q(z) = Q_M e^{-a(T(z)-T_s)}. \quad (7)$$

Here Q_M is the seismic quality factor of the uppermost ice, $T_s = -17.5°C$, the modeled temperature of the ice at $Z = 0.1$ depth in the vicinity of our seismic site [*Funk et al.*, 1994], $T(z)$ is our modeled temperature, and a is a constant that accounts for the physical properties of the ice. Given the observed surface flow velocities of ~200 m a^{-1} at our site [*Horgan et al.*, 2008], and preliminary seismic amplitude analysis suggesting a thawed bed (where $T = -1.4°C$, the pressure melting point for that thickness of pure ice), we modeled the resultant $T(z)$ for each Q value (Figure 6 and Table 2). In order to estimate a, we used only the two well-known temperature values: that at the surface and that at the base of the ice sheet. From these and our Q estimates at those locations, we calculated $a = 0.142°C^{-1}$.

[28] We find an excellent fit between our estimates of temperature and the published englacial temperature measurements and models along the upper reaches of Jakobshavn Isbrae [*Iken et al.*, 1993; *Funk et al.*, 1994; *Lüthi et al.*, 2002; *Poinar and Joughin*, 2010], with our Q-derived englacial temperatures generally within 2°C of these published temperature profiles. Our data do not exhibit a perfect fit to any one profile, which may arise from a bias in our estimate of a, the exact positioning of these temperature profiles within the trough of Jakobshavn Isbrae in relation to our seismic experiment, or modeling uncertainties, particularly near the base of the ice column. Regardless, our Q-derived temperature measurements show close agreement with these temperature profiles, particularly within the lowermost 14% of the ice column, where a temperate basal ice layer is inferred to exist [*Iken et al.*, 1993; *Funk et al.*, 1994; *Lüthi et al.*, 2002; *Poinar and Joughin*, 2010].

[29] We propagate our estimates of uncertainties in Q to uncertainties in T and find that they range from $\sigma_T = 0.8°C$ to $\sigma_T = 2.6°C$ (Table 2). Clearly, if we had used a different temperature profile as a target, such as one of the modeled ones, we would have obtained slightly different results. Nonetheless, the similarity of plausible temperature trends and our Q trend indicates a close correspondence.

[30] The accuracy with which Q can be used to estimate T is dependent on the SNR of seismic reflectors and the distance between reflectors. A high SNR of the reflectors

bounding a given interval of ice will lead to low σ_Q and subsequent low σ_T; this is the case for most of the reflectors we observe. The ice layers with the highest uncertainties are likely the result of the seismic reflectors being spaced too closely to each other; this results in some cross contamination of the frequency spectra of the nearby reflectors (a $\pm$30 ms time window is used in the spectral analysis). Reducing this window to avoid this cross contamination would make estimation of the spectra difficult.

[31] Our attenuation values as a function of temperature are consistent with results of other studies, as shown in Table 1. We note, however, that our use of the known surface and bed temperatures allows smaller uncertainties than is possible from the *a priori* knowledge of $Q(T)$ based on Table 1. Fortunately, the seismic observations reported here can be coupled with other seismic techniques such as amplitude variation with offset (AVO) approach [e.g., *Peters et al.*, 2007; *Peters*, 2009], that are efficient for identifying frozen versus thawed beds, thus providing accurate basal temperatures for thawed beds or a useful limit for frozen beds.

[32] As discussed above, in cold ice the attenuation is sensitive to *c* axis fabric. However, although the reflectors we use likely arise from contrasts in *c* axis fabric [*Bennett*, 1968; *Bentley*, 1971b; *Blankenship and Bentley*, 1987; *Horgan et al.*, 2008, 2011], they occur at sufficiently high temperature where attenuation is primarily controlled by temperature. A sufficiently large suite of analyses such as ours might allow identification of subtle effects arising from variations in *c* axis fabrics, impurity content, or perhaps other factors [e.g., *Alley et al.*, 1995]; however, we anticipate that temperature will be the major control on attenuation in most cases.

6. Summary

[33] We have applied the spectral ratio method to seismic data acquired on Jakobshavn Isbrae, Greenland in order to calculate seismic quality factor $Q(z)$. The decrease of Q with depth is most likely due to an increase in temperature with depth. Comparison of $Q(z)$ to englacial temperature profiles and models [*Iken et al.*, 1993; *Funk et al.*, 1994; *Lüthi et al.*, 2002; *Poinar and Joughin*, 2010] results in an excellent correspondence, suggesting that seismic attenuation can be used as an englacial thermometer.

[34] This surface-based approach for inferring englacial temperature could prove broadly useful, providing modelers with data to test and tune models. A sufficiently large data set, tied to the existing borehole profiles, may allow absolute estimation of temperature directly from Q without independent knowledge of basal temperature, which in turn would allow improved assessment of geothermal flux and its implications for tectonic history of the ice-covered regions of the world. Improving our understanding of seismic attenuation in ice will also give seismologists the ability to better characterize subglacial materials. This method would especially be advanced by collecting more seismic data collocated with englacial temperature profiles, as well as in situ borehole measurements of seismic attenuation through the ice column, to increase the quantity and accuracy of data relating seismic attenuation to temperatures and other factors in glacial ice.

[35] **Acknowledgments.** We would like to thank H. J. Horgan, G. P. Tsoflias, and J. P. Winberry for field assistance in collecting the seismic data presented and analyzed here, along with field support from VECO Polar Services and Air Greenland. We thank CReSIS for the Jakobshavn Isbrae bed elevation data set collected by S. Gogineni et al., using airborne ice-penetrating radar with support from the National Science Foundation (NSF-OPP-0122520) and the National Aeronautics and Space Administration (NASA-NAG5-12659 and NASA-NAG5-12980). We also thank Alessio Gusmeroli, Martin Lüthi, and Andrew M. Smith for constructive reviews that improved the manuscript. Funding for this work was provided by the National Science Foundation (NSF-ANT-1043675) and the Center for Remote Sensing of Ice Sheets (CReSIS) (NSF-OPP-0424589).

References

Aki, K., and P. G. Richards (2002), *Quantitative Seismology*, 2nd ed., Univ. Sci., Sausalito, Calif.

Alley, R., A. Gow, and D. Meese (1995), Mapping *c*-axis fabrics to study physical processes in ice, *J. Glaciol.*, *47*(137), 197–203.

Artemieva, I. M., M. Billien, J. Lévêque, and W. D. Mooney (2004), Shear wave velocity, seismic velocity, and thermal structure of the continental upper mantle, *Geophys. J. Int.*, *157*, 607–628.

Bamber, J., R. Layberry, and S. Gogineni (2001), A new ice thickness and bed data set for the Greenland ice sheet: 1. Measurement, data reduction, and errors, *J. Geophys. Res.*, *106*(D24), 33,773–33,780, doi:10.1029/2001JD900054.

Bennett, H. F. (1968), An investigation into velocity anisotropy through measurements of ultrasonic wave velocities in snow and ice cores from Greenland and Antarctica, PhD thesis, Univ. of Wis.-Madison, Madison.

Bentley, C. R. (1971a), Seismic evidence for moraine within the basal Antarctic ice sheet, in *Antarctic Snow and Ice Studies II*, *Antarct. Res. Ser.*, vol. 16, edited by A. P. Crary, pp. 89–129, AGU, Washington, D. C.

Bentley, C. R. (1971b), Seismic anisotropy in the West Antarctic ice sheet, in *Antarctic Snow and Ice Studies II, Antarct. Res. Ser.*, vol. 16, edited by A. P. Crary, pp. 131–177, AGU, Washington, D. C.

Bentley, C. R., and H. Kohnen (1976), Seismic refraction measurements of internal friction in Antarctic ice, *J. Geophys. Res.*, *81*, 1519–1526, doi:10.1029/JB081i008p01519.

Best, A. I., J. Sothcott, and C. McCann (2007), A laboratory study of seismic velocity and attenuation anisotropy in near-surface sedimentary rocks, *Geophys. Prospect.*, *55*, 609–625.

Blankenship, D. D., and C. R. Bentley (1987), The crystalline fabric of polar ice sheets inferred from seismic anisotropy, in *The Physical Basis of Ice Sheet Modelling*, *IAHS Publ.*, *170*, 17–28.

Brockamp, B., and H. Kohnen (1965), Ein Beitrag zu den seismischen Unterschungen auf dem Gröenändischen Inlandeis, *Polarforschung*, *6*, 2–12.

Chinchinina, T. I., I. R. Obolentseva, and G. Ronquillo-Jarillo (2009), Anisotropy of seismic attenuation in fracture media: Theory and ultrasonic experiment, *Transp. Porous Media*, *79*, 1–14.

Clee, T. E., J. C. Savage, and K. G. Neave (1969), Internal friction in ice near its melting point, *J. Geophys. Res.*, *74*(4), 973–980, doi:10.1029/JB074i004p00973.

Cuffey, K. M., and W. S. B. Paterson (2010), *The Physics of Glaciers*, 4th ed., Elsevier, New York.

Dahl-Jensen, D., K. Mosegaard, N. Gundestrup, G. D. Clow, S. J. Johnsen, A. W. Hansen, and N. Balling (1998), Past temperature directly from the Greenland ice sheet, *Science*, *282*, 268–271.

Dasgupta, R. (1994), Seismic wave attenuation with respect to reflection seismology, PhD thesis, Univ. of Leeds, Leeds, U. K.

Dasgupta, R., and R. A. Clark (1998), Estimation of *Q* from surface seismic reflection data, *Geophysics*, *63*(6), 2120–2128.

Dash, J. G., H. Fu, and J. S. Wettlaufer (1995), The premelting of ice and its environmental consequences, *Rev. Mod. Phys.*, *58*, 115–167.

Dash, J. G., A. W. Rempel, and J. S. Wettlaufer (1996), The physics of premelted ice and its environmental consequences, *Rev. Mod. Phys.*, *78*(3), 695–741.

Engelhardt, H. (2004), Thermal regime and dynamics of the West Antarctic ice sheet, *Ann. Glaciol.*, *39*, 85–92.

Funk, M., K. Echelmeyer, and A. Iken (1994), Mechanisms of fast flow in Jakobshavn Isbrae, Greenland; part II: Modeling of englacial temperatures, *J. Glaciol.*, *40*, 569–585.

Greve, R. (1997), Application of a polythermal three-dimensional ice sheet model to the Greenland ice sheet: Response to steady-state and transient climate scenarios, *J. Clim.*, *10*, 901–918.

Gusmeroli, A., R. A. Clark, T. Murray, A. D. Booth, B. Kulessa, and B. E. Barrett (2010), Seismic wave attenuation in the uppermost glacier ice of Storglaciären, Sweden, *J. Glaciol.*, *56*(196), 249–256.

Hooke, R. L. (1981), Flow law for polycrystalline ice in glaciers: Comparison of theoretical predictions, laboratory data, and field measurements, *Rev. Geophys.*, *19*(4), 664–672.

Horgan, H. J., S. Anandakrishnan, R. B. Alley, L. E. Peters, G. P. Tsoflias, D. E. Voigt, and J. P. Winberry (2008), Complex fabric development revealed by englacial seismic reflectivity: Jakobshavn Isbrae, Greenland, *Geophys. Res. Lett.*, *35*, L10501, doi:10.1029/2008GL033712.

Horgan, H. J., S. Anandakrishnan, R. B. Alley, P. G. Burkett, and L. E. Peters (2011), Englacial seismic reflectivity: Imaging crystal-orientation fabric in West Antarctica, *J. Glaciol.*, *57*(204), 639–650.

Huybrechts, P., and J. Oerlemans (1988), Evolution of the East Antarctic ice sheet: A numerical study of thermo-mechanical response patterns with changing climate, *Ann. Glaciol.*, *11*, 52–59.

Iken, A., K. Echelmeyer, W. Harrison, and M. Funk (1993), Mechanisms of fast flow in Jakobshavn Isbrae, West Greenland; part I: Measurements of temperature and water level in deep boreholes, *J. Glaciol.*, *39*, 15–25.

Jackson, I., M. S. Paterson, and J. D. Fitz Gerald (1992), Seismic wave dispersion and attenuation in Åheim dunite: An experimental study, *J. Geophys. Int.*, *108*, 517–534.

Jarvis, E. P., and E. C. King (1993), The seismic wavefield recorded on an Antarctic ice shelf, *J. Seismic Explor.*, *2*, 69–86.

Joughin, I., et al. (2005), Continued deceleration of Whillans Ice Stream, West Antarctica, *Geophys. Res. Lett.*, *32*, L22501, doi:10.1029/2005GL024319.

Kohnen, H. (1969), Über die Absorption elastischer longituninaler Wellen im Eis, *Polarforschung*, *39*, 269–275.

Kohnen, H. (1974), The temperature dependence of seismic waves in ice, *J. Glaciol.*, *13*, 144–147.

Kuroiwa, D. (1964), Internal friction of ice, *Contrib. Inst. Low Temp. Sci. Hokkaido Univ., Ser. A*, *18*, 1–24.

Kuroiwa, D., and K. Yamaji (1959), Internal friction in polycrystalline and single-crystal ice, *Contrib. Inst. Low Temp. Sci. Hokkaido Univ., Ser. A*, *18*, 97–114.

Langleben, M. P. (1969), Attenuation of sound in sea ice, 10–500 kHz, *J. Glaciol.*, *8*(54), 399–406.

Lüthi, M., M. Funk, A. Iken, S. Gogenini, and M. Truffer (2002), Mechanisms of fast flow in Jakobshavn Isbrae, West Greenland; part III: Measurements of ice deformation, temperature, and cross-borehole conductivity in boreholes to bedrock, *J. Glaciol.*, *48*, 369–385.

Matas, J., and M. S. T. Bukowinski (2007), On the anelastic contribution to the temperature dependence of lower mantle seismic velocities, *Earth Planet. Sci. Lett.*, *259*, 51–65.

Matsushima, J., M. Suzuki, Y. Kato, T. Nibe, and S. Rokugawa (2008), Laboratory experiments of compressional ultrasonic wave attenuation in partially frozen brines, *Geophysics*, *73*(2), N9–N18.

Mavko, G. M., and A. Nur (1979), Wave attenuation in partially saturated rocks, *Geophysics*, *44*(2), 161–178.

Millecamps, R., and M. Lafargue (1957), Sur la propagation des ultrasons dans un glacier, *C. R. Acad. Sci., Ser. B*, *244*, 2824–2827.

Oguro, M., K. Hatano, and S. Kato (1982), Orientation dependence of internal friction in artificial crystals of ice, *Cold Reg. Sci. Technol.*, *6*, 29–35.

Parizek, B. R., and R. B. Alley (2004), Implications of increased Greenland surface melt under global-warming scenarios: Ice-sheet simulations, *Quat. Sci. Rev.*, *23*, 1013–1027.

Parizek, B. R., R. B. Alley, and D. R. MacAyeal (2005), The PSU/UofC finite-element thermomechanical flowline model of ice-sheet evolution, *Cold Reg. Sci. Technol.*, *42*, 145–168.

Paterson, W. S. B., and G. K. C. Clarke (1978), Comparison of theoretical and observed temperature profiles in Devon Island Ice Cap, Canada, *Geophys. J. R. Astron. Soc.*, *55*, 615–632.

Payne, A. J., et al. (2000), Results from the EISMINT model intercomparison: The effects of thermomechanical coupling, *J. Glaciol.*, *46*(153), 227–238.

Peters, L. E. (2009), A seismic investigation of basal conditions in glaciated regions, PhD thesis, Pa. State Univ., University Park.

Peters, L. E., S. Anandakrishnan, R. B. Alley, and A. M. Smith (2007), Extensive storage of basal meltwater in the onset region of a West Antarctic ice stream, *Geology*, *35*(3), 251–254, doi:10.1130/G23222A.

Poinar, K. E., and I. Joughin (2010), Temperate ice under Jakobshavn Isbrae and other Greenland glaciers, Abstract C23B-0606 presented at 2010 Fall Meeting, AGU, San Francisco, Calif., 13–17 Dec.

Robin, G. de Q. (1955), Ice movement and temperature distribution in ice sheets and glaciers, *J. Glaciol.*, *2*, 523–532.

Robin, G. de Q. (1958), *Glaciology III, Seismic Shooting and Related Investigations*, Norsk Polarinst., Oslo.

Rothlisberger, H. (1972), *Seismic Exploration in Cold Regions, Cold Reg. Sci. Eng. Monogr.*, vol. 2, U.S. Army Cold Reg. Res. and Eng. Lab., Hanover, N. H.

Shearer, P. (2009), *Introduction to Seismology*, 2nd ed., Cambridge Univ. Press, Cambridge, U. K.

Spetzler, H., and D. L. Anderson (1968), The effect of temperature and partial melting on velocity and attenuation in a simple binary system, *J. Geophys. Res.*, *73*(18), 6051–6060.

Spetzler, J., and R. Sneider (2004), The Fresnel volumes and transmitted waves, *Geophysics*, *60*, 653–663.

Töksoz, M. N., and D. H. Johnston (Eds.) (1981), *Seismic Wave Attenuation*, Soc. of Explor. Geophys., Tulsa, Okla.

Töksoz, M. N., D. H. Johnston, and A. Timur (1979), Attenuation of seismic waves in dry and saturated rocks: I. Laboratory measurements, *Geophysics*, *44*(4), 681–690.

Tonn, R. (1991), The determination of seismic quality factor *Q* from seismic data, *Geophys. Prospect.*, *39*, 1–27.

van der Veen, C. J., T. Leftwich, R. von Frese, B. M. Csatho, and J. Li (2007), Subglacial topography and geothermal heat flux: Potential interactions with drainage of the Greenland ice sheet, *Geophys. Res. Lett.*, *34*, L12501, doi:10.1029/2007GL030046.

Weertman, J. (1968), Comparison between measured and theoretical temperature profiles at the Camp Century, Greenland, borehole, *J. Geophys. Res.*, *73*(8), 2691–2700, doi:10.1029/JB073i008p02691.

Westphal, J. (1965), In situ acoustic attenuation measurements in glacial ice, *J. Geophys. Res.*, *70*(8), 1849–1853, doi:10.1029/JZ070i008p01849.

R. B. Alley, S. Anandakrishnan, L. E. Peters, and D. E. Voigt, Department of Geosciences, Pennsylvania State University, University Park, PA 16802, USA. (lpeters@geosc.psu.edu)